HELICOPTER ROTOR BLADE AEROACOUSTICS:
A COMPARISON OF MODEL-SCALE WIND TUNNEL AND FULL-SCALE FLIGHT TEST RESULTS

H. Heller, H. Buchholz, K.-J. Schultz, S.R. Ahmed, W. Splettstoesser

Deutsche Forschungsanstalt für Luft- und Raumfahrt, DLR
Institut für Entwurfsaerodynamik, Abteilung Technische Akustik
Braunschweig, Germany

Abstract

Several major international-cooperative rotor-aeroacoustics research programs have been conducted during the past decade, employing a 40% geometrically and dynamically scaled model of the main rotor of an ECD (MBB respectively) helicopter BO-105, most notably the European Brite/ Euram HELINOISE project and the European/US HART-project. Among several other objectives, these projects served to simultaneously determine unsteady blade surface pressures and the resulting acoustic radiation and to provide a comprehensive data bench. A wealth of information was obtained to be used for both validating and furthering rotor noise prediction schemes but also to devise means to reduce noise at the source. Although the model scaling factor was large (namely 0.4) thus implying a good scalability towards the full-scale condition, the final proof was still lacking, in that no comparable aeroacoustics information from the full-scale "counter-part" of the model rotor was available. In view of this deficiency, a first dedicated flight experiment was initiated employing DLR's BO-105 helicopter one of whose main rotor blades was equipped with a number of flush-mounted dynamic pressure sensors. The test helicopter was flown at nominally identical conditions as had previously been simulated in the wind tunnel such as climb, level flight, and moderate speed descent (with strong blade vortex interaction impulsive noise occurring). This paper reports about initial results towards comparing model and full-scale flight test (a) unsteady blade pressures, and (b) acoustic nearfield radiation (for one location under the advancing rotor side employing a fuselage-mounted microphone). In general, the operational conditions (especially the flight path angles) were found to slightly differ for full-scale and model scale for a best agreement of the blade pressures and also of the acoustic data. The likely reasons are discussed.

List of Symbols

C	blade chord, m
C_p	pressure coefficient = $p/(0.5\,\rho\,[V \sin\psi + r\,\omega]^2)$
C_T	thrust coefficient = $T/(\pi\,\rho\,\omega^2\,R4)$
F	constant
M_H	hover Mach number
p	blade surface pressure, N/m^2
R	rotor diameter, m
r	rotor spanwise coordinate, m
T	rotor thrust, N
V	flow speed, flight speed, m/s
x	rotor chord coordinate, m
α_{TPP}	rotor tip path plane angle, degree
Θ_{FT}	flight path angle for the flight test, degree
Θ_{WT}	„flight path" angle in the wind tunnel, degree
μ	advance ratio = $V/R\omega$
ψ	rotor rotational azimuthal angle, degree
ρ	air density, kg/m^3
ω	rotor angular velocity, 1/s

1. Introduction

Of all flight noise contributors, the helicopter is probably the single most offensive on account of its acoustically highly disturbing characteristics, most notably the well known „slapping noise" which occurs during high speed flight and moderate speed descent. These characteristics make helicopter noise not only detectable over large distances but also highly annoying and intrusive. Consequently, helicopter noise - more specifically the noise of helicopter rotors - has been the subject of intense research efforts, dating back to the early eighties.

During the past decade a number of very comprehensive, international-cooperative, and largely experimental research projects have been executed, probing into the very source mechanisms of rotor noise. It was recognized that only by fully understanding the complex interaction of rotor blade dynamics and rotor blade aerodynamics would it be possible to accurately predict and eventually control rotor noise.

Understanding rotor noise hinges on understanding the unsteady aerodynamics on and near a rotor blade. Here the unsteady blade surface pressures in their dependence on rotor geometry, rotor elasticity and rotor operational conditions, constitute a key parameter. Of the three rotor source mechanisms (or source types), namely *thickness noise*, *loading noise* and *quadrupole noise*, loading noise (also termed force noise) can be determined on the basis of Lighthill's acoustic analogy approach (as rewritten by Ffowcs Williams and Hawkings) if, among several other pertinent parameters, the unsteady blade surface pres-

sures are accurately known. Calculating quadrupole noise requires information on the unsteady velocity field close to the rotor blade, although approximate methods have been developed to determine quadrupole noise using blade surface pressure information. Only thickness noise can be determined in a rather straight forward manner solely from rotor geometrical and rotor operational inputs.

Recognizing the importance of unsteady blade pressure information in understanding the physics of rotor noise resulted in the planning and execution of dedicated experimental projects which made use of modern rotor test facilities (model rotors) and excellent acoustic wind tunnels, most notably the German Dutch Wind Tunnel, DNW.

Details of such work conducted in the DNW have been reported by Boxwell et al. [1], Splettstoesser et al. [2], Dadone et al. [3], Zinner et al. [4], Schultz et al. [5], Liu et al. [6], and Lorber [7]. Model rotor tests conducted in the French Modane S1 Wind Tunnel are reported by Polacsek [8]. Few flight test projects with instrumented rotor blades have occurred so far. Westland Helicopter studied blade stall mechanisms on the BERP-blade of the Lynx helicopter, as reported by Isaacs [9] and within a NASA/US-Army flight test a UH-60 helicopter with instrumented rotor blades was employed [10], all data not openly available to the research community.

One of the most comprehensive such projects has been conducted in the framework of the EC (now EU) launched research initiative Brite/Euram in 1990. Here, in an 8-nation cooperative research effort high quality aeroacoustic data were obtained on a BO-105 helicopter model main rotor in the DNW. The project under the acronym HELINOISE[1] for the first time provided simultaneously measured unsteady blade surface pressures and acoustic radiation over the entire operational regime of the main rotor of the datum-helicopter. The results of the HELINOISE project are well documented (e.g. Splettstoesser et al. [11, 12] or Heller et al. [13]).

Although the model scaling factor of the HELINOISE-tests was large (namely 0.4) thus implying a good scalability towards full-scale, the final proof of the validity of the data and their transfer to a realistic flight vehicle situation was still lacking in that no comparable aeroacoustics information employing the „full-scale counterpart" of the model rotor was available. In view of this deficiency, a first dedicated experiment was conducted employing the DLR BO-105 helicopter one of whose main rotor blades was equipped with a number of flush-mounted dynamic pressure sensors.

In addition the flight test helicopter carried a fuselage-mounted microphone to acquire nearfield acoustic radiation data. Such data, at corresponding locations, had been obtained during the HELINOISE experiment.

In the following selected results on comparing (a) unsteady blade pressures, and (b) nearfield noise at one location under the rotor advancing side, from model and full-scale flight tests for climb, level flight and descent (with strong blade vortex interaction, BVI, impulsive noise occurring) are presented and discussed, attempting to find answers to the following questions

- Can operational parameters of wind tunnel and flight tests be matched in such a way as to duplicate the physics of noise generation and radiation in both cases?
- Are there conditions where a precise matching is not so essential, and are there others where even minor deviations lead to grossly differing results?
- How good is the agreement of blade pressure and acoustic radiation data obtained in wind tunnel model and in flight tests?

2. Wind Tunnel Model Tests - The HELINOISE Project

The experimental specifics and results of the HELINOISE project have been discussed in depth (e.g. Splettstoesser et al. [11, 12]). Since blade surface pressure and acoustic radiation data of the HELINOISE project will be used in the comparison with the subject flight test data, some essential information is presented in the following.

2.1 The German Dutch Wind Tunnel

The rotor model tests were conducted in the German Dutch Wind Tunnel, DNW, in its open test section anechoic configuration. The DNW's technical features are well documented (e.g. van Ditshuizen et al. [14]). The flow emanates from the 6 by 8 m open nozzle through the anechoic test hall of 30.000 m³ across a distance of 19 m towards the 9.5 by 9.5 m collector. Due to the large unobstructed volume of the test hall, and the flow cross-section of initially 6 x 8 m, fairly large models of rotors can be accomodated still entirely within the clean tunnel jet flow.

2.2 Test Rig and Model Rotor

The HELINOISE rotor test stand to drive test rotors is well documented (e.g. Stephan et al. [15]) where details about its hydraulic drive system (power capability 130 kW), its rotor balance and its rotor control system are given. The drive system is housed in a noise-reducing fairing approximately shaped like a helicopter fuselage. The test rig is attached to a hydraulically actuated model sting, allowing to tilt the rotor tip path plane. In combination with the variable tunnel flow („flight") speed (up to 80 m/s) any desired flight condition can be readily simulated. The rotor is supported in „mid air", permitting

[1] Subsequent research projects, such as the European HELISHAPE-project and the European/US HART-project extended the HELINOISE tests towards other rotors and towards the effects on noise and vibration of higher harmonic blade control

completely unobstructed sound propagation into the free field environment for acoustic measurements in a large regime around the rotor.

The model rotor itself is a 40% geometrically and dynamically scaled model of the 4-blade hingeless BO-105 main rotor. The photograph (Fig. 1) shows the set-up in the DNW. The rotor has a diameter of 4 m (vs. the full-scale 9.82 m diameter). The rotor blades feature a NACA 23012 airfoil with a -8° linear twist, a square tip and a solidity of 0.077. Nominal rotor operational speed is 1040 rpm, giving an acoustic blade passage frequency of about 70 Hz. The nominal hover tip Mach number is 0.641. The glass-fiber reinforced plastic rotor blades have similar mass and stiffness distribution as the full-scale rotor, providing acceptable matching of the blade natural frequencies for the first few modes of inplane, flapwise and torsional motion.

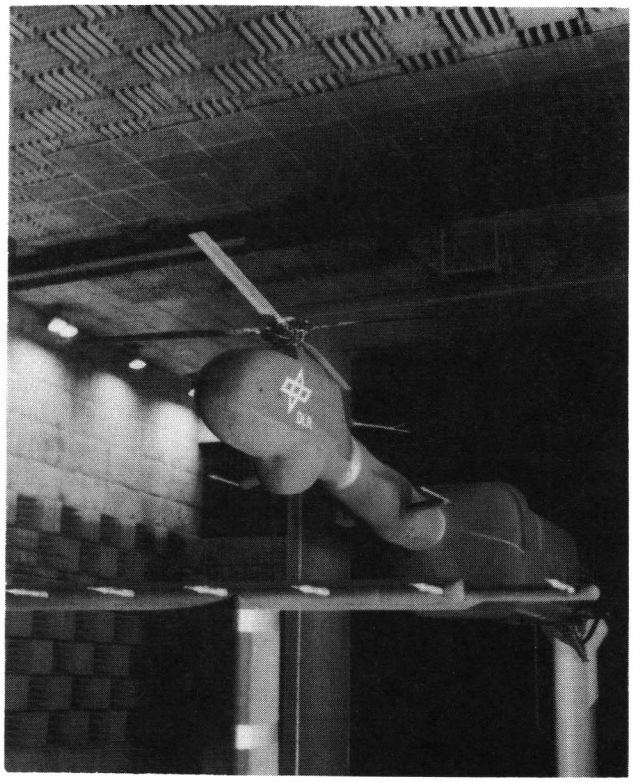

Fig. 1 Setup for rotor aeroacoustics tests in the DNW

2.3 Instrumentation and Layout

2.3.1 Blade-mounted Pressure Sensors

124 specially designed KULITE LQ-32-064-25A miniature absolute pressure sensors (measuring range up to 170 kPa) were installed in one of the rotor blades at locations shown in Fig. 2. Accordingly, 3 radial sections at, respectively, r/R = 75%, 87% and 97% were heavily instrumented both on the upper and the lower blade surface, while at 6 additional radial stations (from 60% to 99%

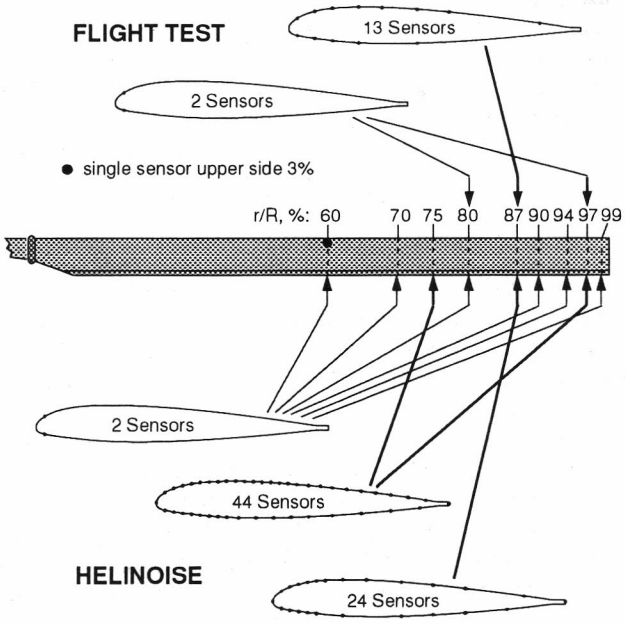

Fig. 2 Sensor distribution on full-scale ("Flight Test") and model ("HELINOISE") rotor blades

radius) there were only 2 sensors close to the blade's leading edge, one on the upper, one on the lower surface.

The sensors were submerged in the blade surface being in contact with the outside pressure field through very short tubes of 0.5 mm inner diameter resulting in a frequency response flat within 1 dB up to 7 kHz.

2.3.2 „Fuselage-mounted" Microphone

Locations of two „fuselage-mounted" microphones to measure acoustic nearfield radiation may be seen in Fig. 1. They were respectively placed under the rotor advancing and rotor retreating sides. However only the „rotor advancing side"-microphone could be installed at the corresponding location on the flight test vehicle.

2.4 Data Acquisition and Processing

Wind tunnel performance data, such as flow speed, flow density, temperature and humidity, and tunnel flow pressure as well as *rotor performance data*, such as rotational speed (blade tip hover Mach number), rotor thrust and tip-path plane inclination were transferred and stored on a common data base for each data point (measurement condition).

The output signals of the 124 pressure sensors were preamplified in the rotating frame and transmitted via a slipring system to the fixed frame and simultaneously sampled at a rate of 2048/rev to provide a useful frequency range in excess of 10 kHz. Raw data for 60 revolutions were stored in transputer memories for subsequent computation of averaged blade pressure time histories and narrow band spectra. Acoustic data from the fuselage

fixed microphones were acquired in the standard manner using both a digital and analog data acquisition chain. All data acquisition systems (for tunnel performance, rotor performance, blade-mounted pressure sensors signals and fixed microphone acoustic data) were linked via Ethernet to provide time-synchronization of rotor operation and ensuing blade pressures and acoustic radiation.

2.5 Test Conduct and Wind Tunnel Correction

2.5.1 Test Matrix

The operational range of a helicopter is characterized in terms of its climb - or descent-rate and its forward speed. These parameters define the climb- or descent-angle. The test matrix of the HELINOISE project (Fig. 3) covered in essence the entire operational regime of the datum helicopter with special emphasis on certain critical flight regimes (e.g. moderate to high speed descent at various rates and high speed level flight) known to give rise to *blade/vortex interaction (BVI)* and *high speed (HS)* impulsive noise. The HELINOISE test matrix was based on the following non-dimensional test parameters (which had to be matched in the flight tests), namely advance ratio μ, thrust coefficient C_T, hover tip Mach number M_H and tip path plane angle α_{TPP}, for the rotor operating in a momentum-free condition [1, 2]. This then was to correspond to the full-scale flight case as defined by flight speed V and flight path angle Θ_{FT}.

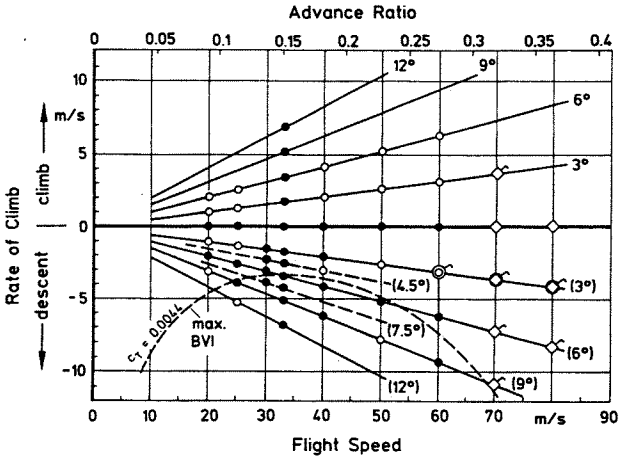

Fig. 3 HELINOISE test matrix

2.5.2 Test Condition Establishment

Operating a model rotor in an open test section wind tunnel causes the incident flow to be deflected more than under free flight conditions by an amount $\Delta\alpha$. An effective corrected angle

$$\alpha'_{TPP} = \alpha_{TPP} + \Delta\alpha$$

can be calculated which would represent that angle in free air corresponding to the tunnel α_{TPP} -value. Based on an analysis by Heyson [16] Brooks [17] has given this correction term as

$$\Delta\alpha = F \tan^{-1} (C_T \cos\alpha_{TPP}/(2\mu^2 - C_T \sin\alpha_{TPP}))$$

with F = -0.20. The full-scale flight path angle Θ_{FT} is related to the effective tip path plane angle (in the tunnel) by the following equation

$$\Theta_{FT} = \alpha'_{TPP} + 0.44\ \mu^2/C_T$$

Here the factor 0.44 takes into account the equivalent flat-plate drag of 1.2 m² of the BO-105 helicopter. Accordingly then, the inclination of the rotor tip path plane in the wind tunnel was set following these specifications, to simulate the full-scale flight conditions as defined by forward flight speed and rate of climb (i.e. the flight path angle).

3. Flight Tests

3.1 The Test Helicopter

The flight tests to determine blade surface pressures and acoustic nearfield radiation were conducted with the BO 105 helicopter of the DLR (Model Number S 123, built in 1974) as shown in Fig. 4. This helicopter of 2300 kg maximum take off mass is equipped with a four blade main and a two blade tail rotor of, respectively, 9.82 m and 1.9 m diameter. Nominal main and tail rotor rotational speeds are 424 min^{-1}, and 2220 min^{-1}, respectively, corresponding to a gear ratio of about 5.3. The blade of the hingeless main rotor features a rectangular tip and a modified NACA 23012 profile with a -8° linear twist and a chord of 0.27 m.

3.2 Instrumentation and Layout

3.2.1 Blade-mounted Pressure Sensors

An available rotor blade set was instrumented by Eurocopter Deutschland (ECD), the manufacturer of the BO 105 helicopter. Eighteen miniature absolute pressure KULITE sensors of the same type as used in the wind tunnel tests were installed in one of the rotor blades at locations indicated in Fig. 2. Accordingly, radial station r/R = 87% was instrumented with 13 sensors distributed over the upper (see photograph, Fig. 5) and lower surface, one sensor each was placed at a chord position of x/C = 3% on the upper and lower surface at two radial stations r/R = 97% and 70% and the remaining senor was put on the upper surface at the same chord position x/C = 3% but at radial stations r/R = 80%.

3.2.2 Fuselage-mounted Microphone

Only one external, fuselage-fixed microphone could be attached to the right-side landing gear (Fig. 6), at a location under the advancing rotor side corresponding to one of those used in the model tests. A 1/2-inch Brüel&Kjaer microphone type 4134 with a standard nose cone was employed for the purpose.

Fig. 4 DLR flight test helicopter BO 105

3.3 Data Acquisition And Processing

The data acquisition and processing system consisted of three major components including the associated sensors: (1) the *Rotor Data Acquisition System*, to process the signals of the blade-mounted sensors, (2) the *Base-data Acquisition Unit* to acquire and store all base data signals (i.e. essentially rotor operational and helicopter attitude data as well as blade pressure data) and (3) the *Microphone Data Acquisition Unit*, a conventional digital tape recorder. Fig 7 provides a schematic of the entire data acquisition system.

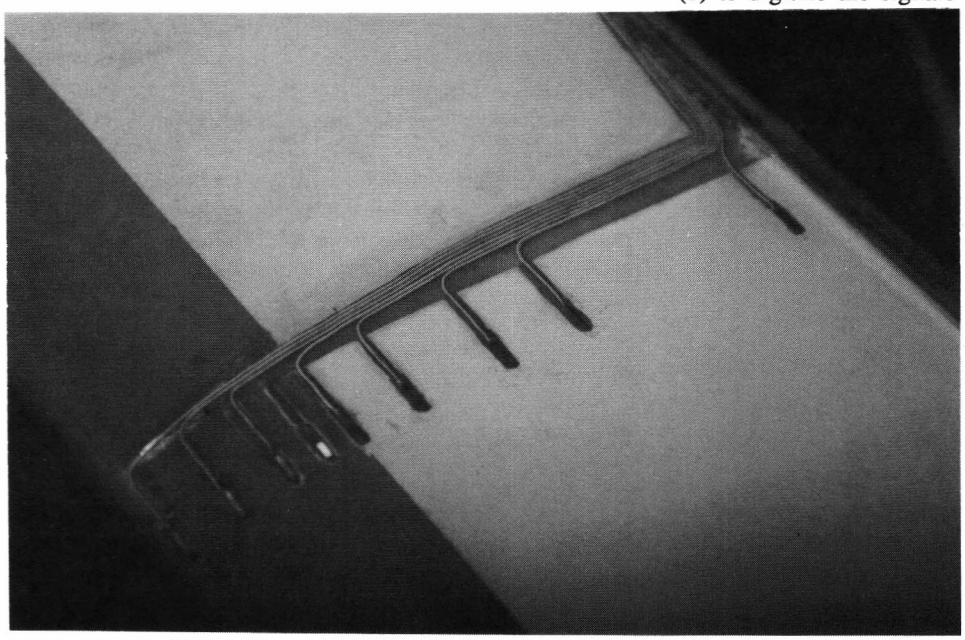

Fig. 5 Photo of upper surface mounted pressure sensors on full scale rotor blade at r/R = 87%

3.3.1 Rotor Data

20 channels of an available 40-channel *Data Acquisition and Processing Unit* could be used providing a sampling rate of 2 kHz with a resolution of 12 bits, corresponding to a rotor azimuthal resolution of 1.35 degrees. The whole unit was encapsulated in a cylindrical container on the rotor hub. In processing, the sensor signals were amplified, transferred to an A/D-converter and either intermittently stored on and transmitted to base unit after each measurement, or directly transferred to the base unit's hard disk storage already during the measurement. A transputer controlled A/D-conversion and data storage, as well as data transmission to the base unit through a link (a very fast serial connection). By using such a transputer the number of connections from the rotating to the fixed (on-board) computer could be restricted to just those for the link and for the sensor voltage supply. A major advantage lies in transmitting the signals in digital form, thus being insensitive to external disturbances.

3.3.2 Base Data

A *Base Data Acquisition and Processing Unit* was used (1) to digitize the signals of the base-data (flight speed, flight height, external temperature, rotor-rpm etc) with a low sampling rate of 50 Hz and (2) to secure the base data as well as the (high-frequency) sensor-pressure data arriving from the link. Both data streams were combined into one and stored on the CPU hard disk.This way, for each data point (measurement point) both the high-frequency sensor signals and the low-frequency operational data were available in a common format, facilitating later analysis.

3.3.3 Microphone Data

Acoustic data from the landing gear attached external microphone were acquired through a digital

tape recorder with a 16-bit resolution and a sampling rate of 20 kHz. To synchronize blade pressure and base data, the start and stop signals for each measurement point was recorded, as was the signal of the main rotor rotational position sensor.

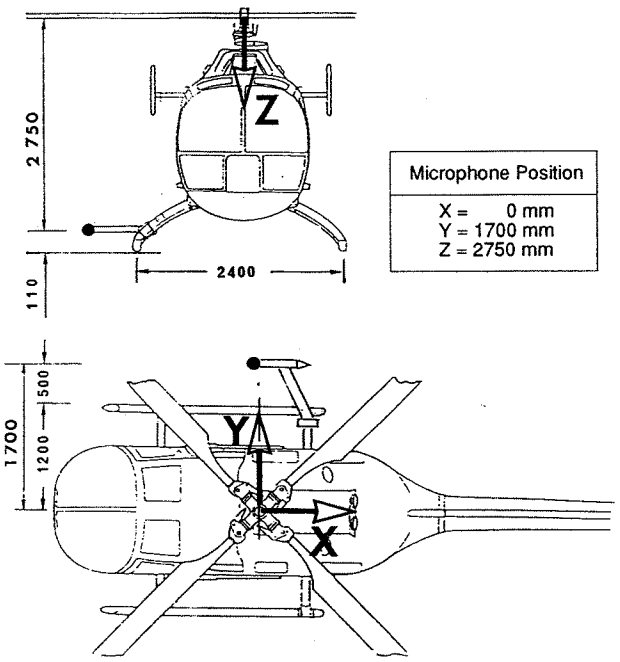

Fig. 6 Location of fuselage mounted microphone

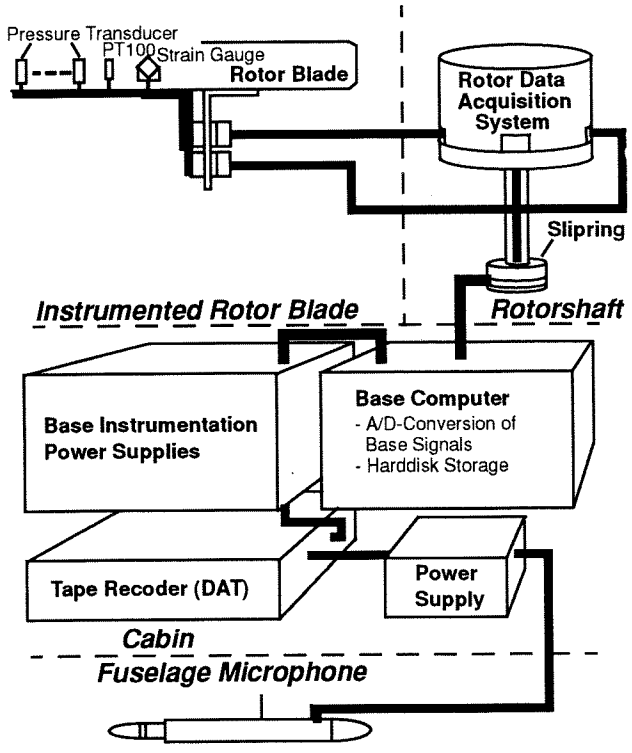

Fig. 7 Data acquisition system for blade surface pressures and acoustic radiation

3.4 Test Conduct

To enable a comparison of wind tunnel and flight test data a test matrix was established for the flight tests to duplicate selected points of the wind tunnel test matrix. Clearly, not all data points could be exactly matched, in particular not those for very high tunnel flow speeds, since the operational flight speed range of the BO-105 is actually much less. Fig. 8 shows the flight test matrix with all data points actually flown.

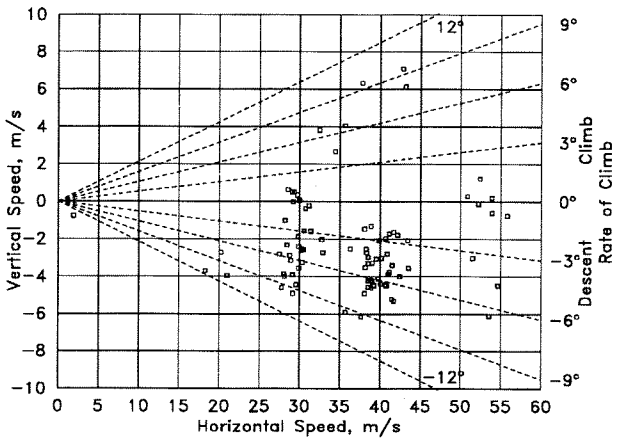

Fig. 8 Test matrix for flight tests

Measurements were conducted in March 1995. Test flight heights lay between 1000 and 1500 ft. Such rather low flight heights were necessary to duplicate the (relatively low) thrust coefficient C_T of typically 0.0044 as used in the DNW-tests which would not be attainable at larger flight altitudes, even though this meant coping with less than ideal weather conditions. Also, realizing this thrust coefficient meant to fly the helicopter near its lowest possible weight (mass). Other than that, test matrix data points could be matched quite well. Since flight speed and flight path deviations from the nominal values were (and in principle are) unavoidable, at least three measurements of several seconds duration each were taken at any nominal flight condition.

Flight operational data, specifically, flight speed and rate-of-climb R/C (positive values => climb, negative values => descent) - i.e. the actual flight path - were determined by means of the onboard cockpit instrumentation, and double-checked with an external "Airspeed and Flow Direction Indicator". This latter instrument operates satisfactorily for flight speeds in excess of approximately 20 m/s. Moreover, it was assumed that if flight speed and flight path angle, as indicated through onboard equipment, corresponded to those taken as the datum conditions in the wind tunnel, then this should result in the same rotor tip path plane inclination with respect to the oncoming flow. Whether this was actually the case was to

be determined from comparing the blade pressure data, considered a very sensitive "litmus-test" towards such an agreement.

3.5 Blade Surface Pressure and Acoustic Data Reduction Specifics

Although it was originally attempted to take any particular flight condition (as defined by its flight speed and climb rate) at its face value and to average blade pressure signals over many consecutive rotor revolutions (and over several seconds) this turned out not being the best approach.

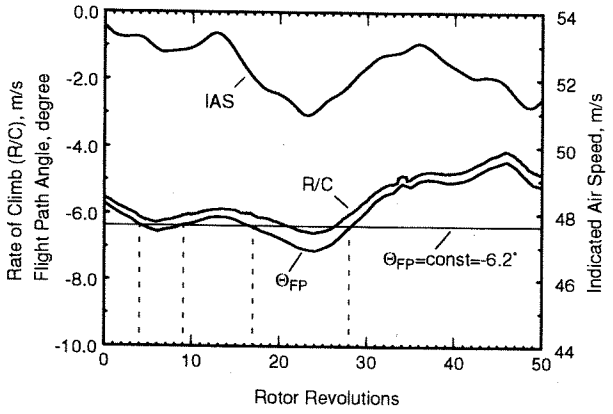

Fig. 9 Flight speed, Rate-of-climb, and Flight-path-angle variations over many rotor revolutions

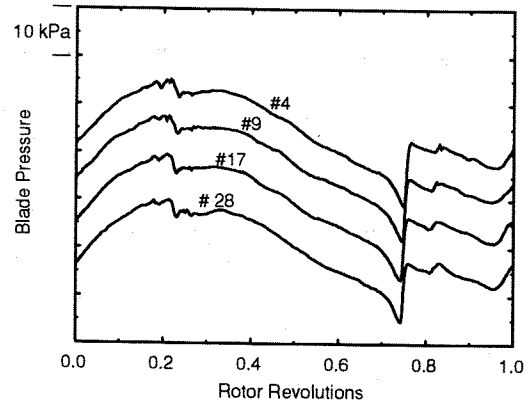

Fig. 10 Blade pressure time histories over one rotor revolution at four nominally identical flight path angles of -6.2° as indicated in Fig. 9

During any given data acquisition time span over several tens of rotor revolutions (typically lasting from 5 to 10 seconds) forward flight speed and rate of climb varied somewhat, as did the ensuing flight path angle. Fig. 9 shows typical variations of these parameters for a nominal 50 m/s forward speed/6°-descent test flight over about 50 rotor revolutions (8 second time duration). Clearly, within that time span the flight speed varied "erratically" between 51 and 53 m/s, approximately, while the flight angle varied between -7° and -5.5° for the first half of that time span and then decreased to values of -4.5° during the remainder. This might appear as rather an erratic flight path, but is evidently quite realistic given actual wind and weather conditions which were not very favorable.

Averaging blade pressure time histories over such a relatively long time duration (with changing rates-of-climb and flight path angles, respectively) would have necessarily led to unacceptable results. Therefore, a search-program was developed where for any nominal flight condition and set measurement duration a pressure time history for just one-rotor-revolution was identified for which the nominal flight conditions were best matched within a predetermined tolerance. In fact, these one-rotor-revolution data set would not necessarily have to stem from the same test flight, as long as the condition of „identical" flight was fulfilled. These several (typically at least 6, frequently more) one-rotor-revolution data were then averaged and taken as the basic result for the selected flight condition.

Recognizing that flight speed variations did not affect the fligh path angle so much, in contrast to the rate-of-climb value, those rotor revolutions were identified where, for example, the flight path angle was within 5.5° and 6.5°. In the test, as illustrated in Fig. 9 this would have meant about 20 rotor revolutions qualifying within this tolerance-criterion. Narrowing down this tolerance criterion to exactly 6.2°, for example, would have led to only 4 individual rotor revolutions qualifying. The corresponding time histories from one sensor for these 4 rotor revolutions obtained within the same test flight but separated by as many as 20 rotor revolutions indicates the feasability of this approach. Indeed, the waveforms - as shown in Fig. 10 - of these four individual time histories (separated for clarity in the ordinate-scale) agree very well with only very minor phase shifts occurring. Accordingly, this data processing methodology was applied in the reducing the test data.

4. Results and Comparisons

4.1 Blade Surface Pressures

The majority of the data to be presented in the following pertains to moderate speed descent cases in regimes where strong blade vortex interaction phenomena occur. In analysing the data it was observed that - in the flight speed range around 30 to 35 m/s - there seemed to be a constant bias between the actual (for the flight tests) and the simulated (for the wind tunnel tests) flight path angles of approximately 3°. Accordingly, model scale wind tunnel data obtained at a certain flight path angle agreed best with those obtained at a 3°-lesser full-scale flight path angle. Hence, in presenting the data both comparisons will be routinely shown, i.e. the blade pressure time

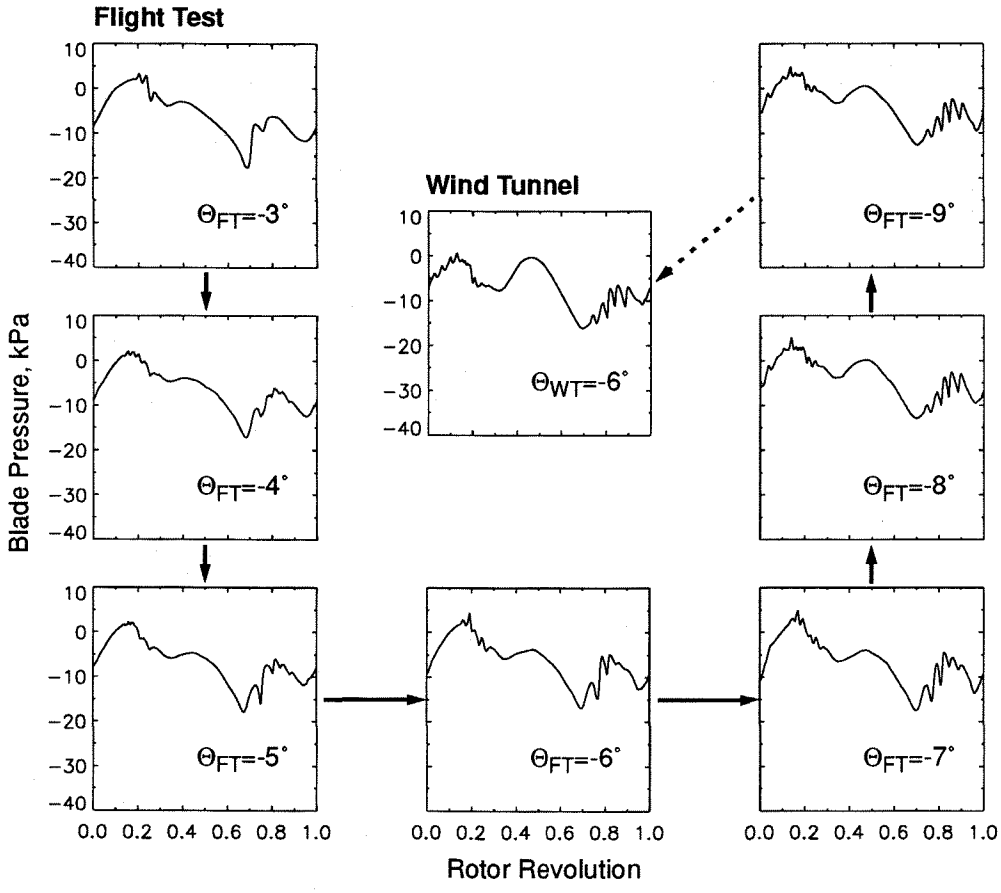

Fig. 11 Comparison of blade pressure time histories for flight path angles ranging from -3° to -9° with one obtained in the wind tunnel at -6°; $V \approx 32$ m/s; $C_T \approx 0.0044$; $M_H \approx 0.641$

histories for the nominally identical flight path angles and for flight path angles different by -3°. Some possible explanations for this behavior will be offered in the discussion further down.

To illustrate the "phenomenon", Fig. 11 shows pressure time histories (PTHs) for a nominal flight speed of 32 m/s and descent angles varying from -3° to -9° in one-degree steps obtained from one upper surface sensor at r/R = 87% and x/C = 3%. Comparing these seven PTHs from the flight tests with the model scale 6°-descent case clearly indicates best agreement for the full-scale 9°-descent case.

4.1.1 Blade Surface PTHs in the Chordwise Direction

Fig. 12 shows blade surface PTHs for one rotor revolution as observed on the upper and the lower blade surface at a blade radial station of r/R = 87% and respectively 3 chordwise positions for a test condition of a nominal 6°-descent at a forward speed of 32 m/s.

As announced above, data are shown for both the identical (i.e. -6°) and the 3°-lesser (i.e. -9°) flight path angle. Clearly, all data reveal the tell-tale sequence of spikes in the first and the fourth rotor quadrant, typical for blade vortex interactions phenomena to be expected under such conditions (and observed and well documented in all previous relevant model scale wind tunnel tests). Again, it appears that the 3°-offset data agree best, as evident from the rather exact coincidence of the BVI-spikes. DC-signal part discrepancies may be expected on account of slight differences in the aeroelastic properties of the full-scale and the model scale rotor blades; moreover, scaling of vortex size is probably not exact, in that core diameters of the full-scale vortices might be smaller than for the model rotor in relative terms. In addition, and probably most significant in this context are the differences in the fuselage geometries which in the model does certainly not fully correspond to the BO-105 fuselage. Finally, there is a tail rotor on the flight vehicle which may affect blade pressures in the downstream location where the fourth and the first rotor quadrant join.

4.1.2 Blade Surface PTHs along the Blade Leading Edge

Fig. 13 shows blade surface PTHs, again for one rotor revolution, for 4 sensors at radial stations r/R = 97%, 87%, 80% and 70% near the leading edge upper surface at x/C = 3% for a constant "flight"-speed of 32 m/s and nominal level flight (0°) and descents with angles 3° and

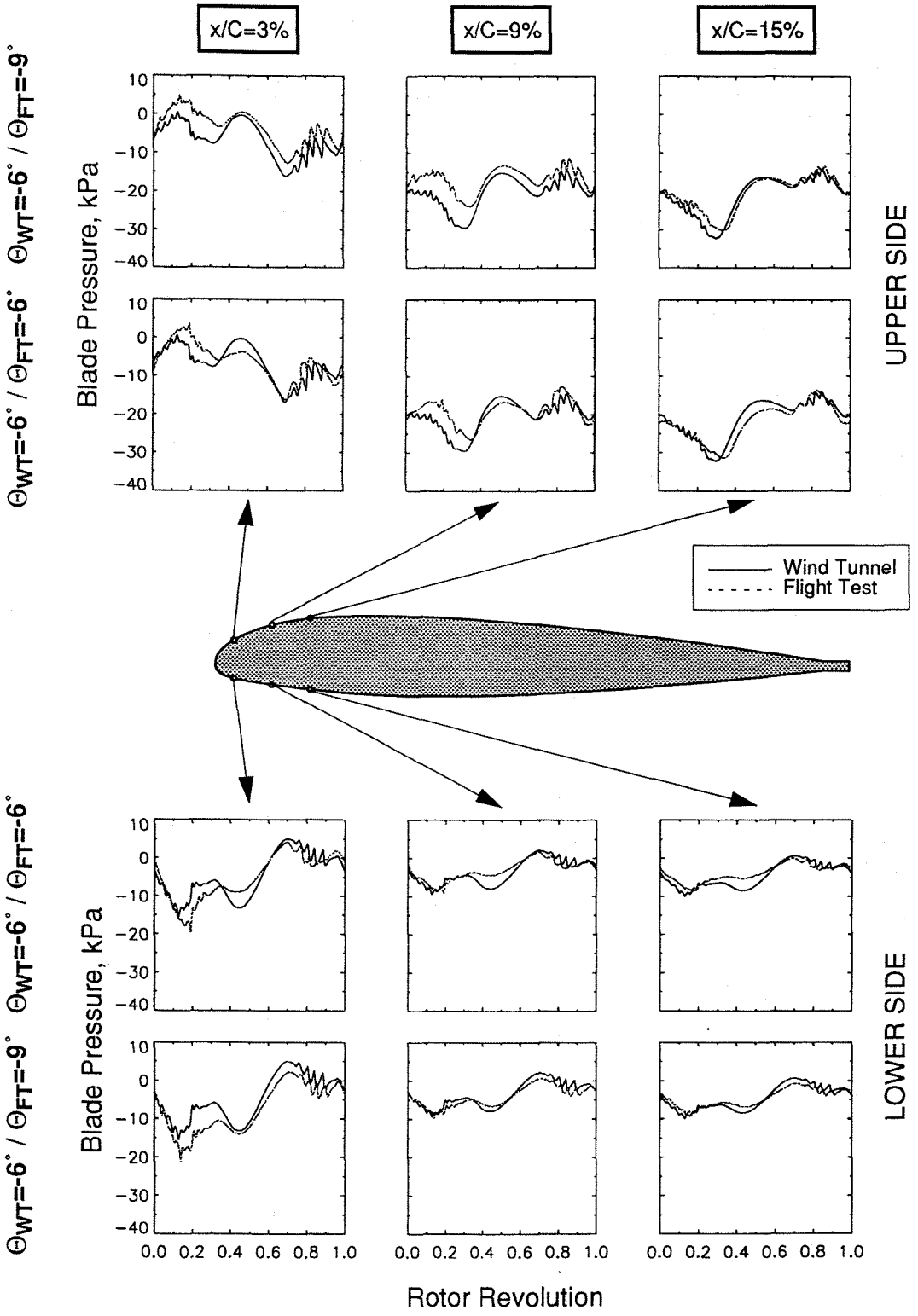

Fig. 12 Blade pressure time histories from wind tunnel and flight tests for different chordwise locations on the upper and lower surface at r/R = 87% and different flight path angles; $V \approx 32$ m/s; $C_T \approx 0.0044$; $M_H \approx 0.641$

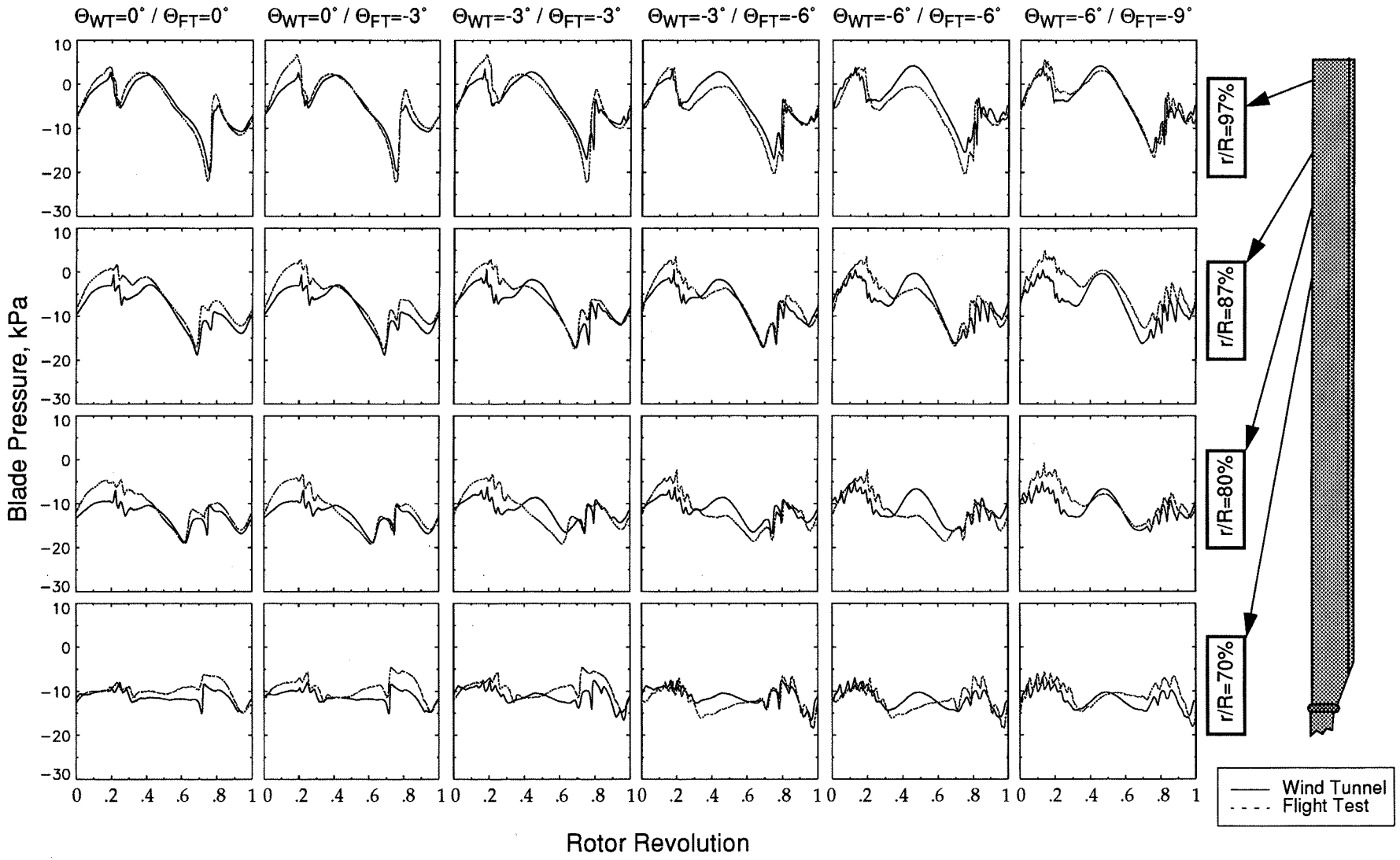

Fig. 13 Blade pressure time histories from wind tunnel and flight tests at several spanwise locations and x/C = 3% on the upper surface at different flight path angles; $V \approx 32$ m/s; $C_T \approx 0.0044$; $M_H \approx 0.641$

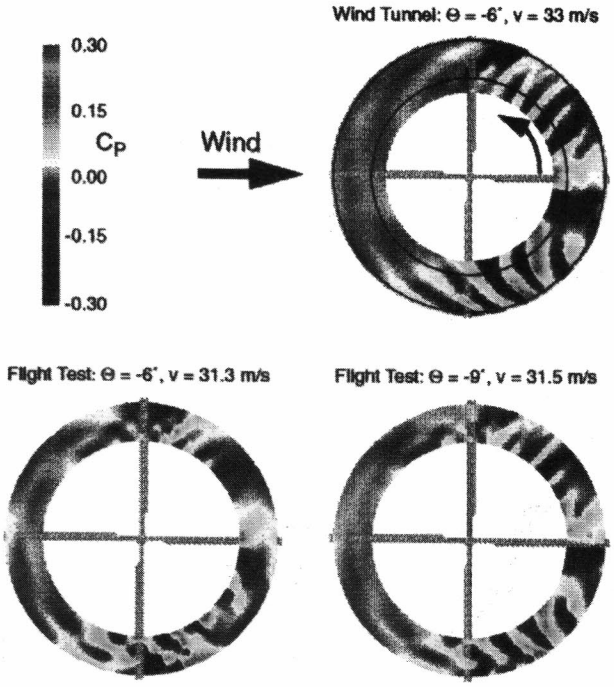

Fig. 14 Blade surface pressures contour plots generated from upper surface leading edge sensor data (x/C = 3%); 6°-descent; V ≈ 32 m/s; $C_T \approx 0.0044$; $M_H \approx 0.641$

6°, respectively. Again data seem to best agree for the 3°-flight angle offset. Following the change in PTH-shape when going from a level flight to a 6°-descent flight condition also shows the growth in BVI-strength with increasing descent angle, evident on all 4 sensor positions. Following the PTHs for the nominal 6°-degree descent condition illustrates the BVI-intensity change in the spanwise direction, revealing at least 6 strong vortex interactions at the more inboard location in the first rotor quadrant, and at least 5 strong interactions at the more outboard location in the fourth quadrant. Hence, BVI-phenomena occurring in flight are remarkably well duplicated in the wind tunnel model tests (or vice versa).

4.1.3 Blade Pressure Contour Plots

This BVI-related agreement is illustrated better still when comparing contour plots of the non-dimensional pressure coefficient C_P, over one revolution, as shown in Fig. 14 again for the case of a moderate speed (32 m/s) nominal 6°-descent. Here the signals from the 4 (flight test) and the 9 (wind tunnel test) leading edge upper surface sensors were used to generate the contour plot clearly revealing the traces of blade vortex interactions in the first (advancing side) and fourth (retreating side) rotor quadrant. In the Figure the top circular plot relates to the model case, the lower two plots to the flight test situation. Here, the left one pertains to a nominal 6°-descent case, whereas the right one to a nominal 9°-descent case, this one revealing an astonishing agreement.

4.1.4 Chordwise Blade Surface Pressure Distribution

Fig. 15 compares the chordwise distribution at a radial station r/R = 0.87 of the pressure coefficient C_P on the upper and lower blade surfaces at fixed rotor azimuthal angles ψ separated by 45°-steps. Again, the moderate speed (32 m/s) case is taken with 6°-descent data for the model scale and 9°-descent data for the flight case. Overall, the agreement is satisfactory, apart from slight deviations at certain azimuthal angles.

4.1.5 Flight Speed Dependence of Blade Surface Pressures

In order to check, whether the observed "3°-flight angle bias" would occur over the entire speed range where data were taken in the flight test, data for nominal flight speeds near 32 m/s, 40 m/s and 51 m/s were compared for a nominal level flight condition and a nominal 3°-descent condition for one upper surface sensor at r/R = 87% and x/C = 3%. Although not every corresponding case could be demonstrated, at least several comparisons are possible, as illustrated in Fig. 16. The data indicate a subtle change in the bias, in that for increasing flight speeds the amount of flight-angle bias seems to decrease. In fact, the high speed level flight frame for identical flight angles of 0° shows better agreement than the one below where tunnel data at 0° are compared with flight data at -3°. Not enough data is presently available to confirm this tendency. However, if that was true then this would point toward a constant bias in the rate-of-climb indication on the flight test vehicle. If that indication was always "wrong" by a constant amount then this would have a graver effect at lower flight speeds than at higher ones.

4.2 Acoustic Radiation

Only very little data was obtained for the acoustic radiation from the rotor at the model-body and helicopter-fuselage, respectively, mounted fixed microphone. It should be understood that for technical reasons the position of these microphones was not optimal considering the major radiation direction for BVI impulsive noise under the advancing rotor in the forward/downward direction. The fixed microphone locations as used in the subject tests were much too close to the fuselage to be able to pick up maximum BVI noise.

Purely to ascertain the degree of agreement between the model and the flight test acoustic radiation results, the data, obtained at the identical scaled locations, could be used nevertheless. Fig. 17 illustrates the results, showing for a nominally "constant" flight/flow speed range of 30 to 33 m/s the acoustic pressure time histories for a nominal 6°-descent, a level flight, and a 6°-climb. Again, data are shown both for the respectively identical flight angle, and for one 3° less (only for the descent and the level flight cases). Although not as clear-cut as for the (much more sensitive) blade pressures, the acoustic data seem to

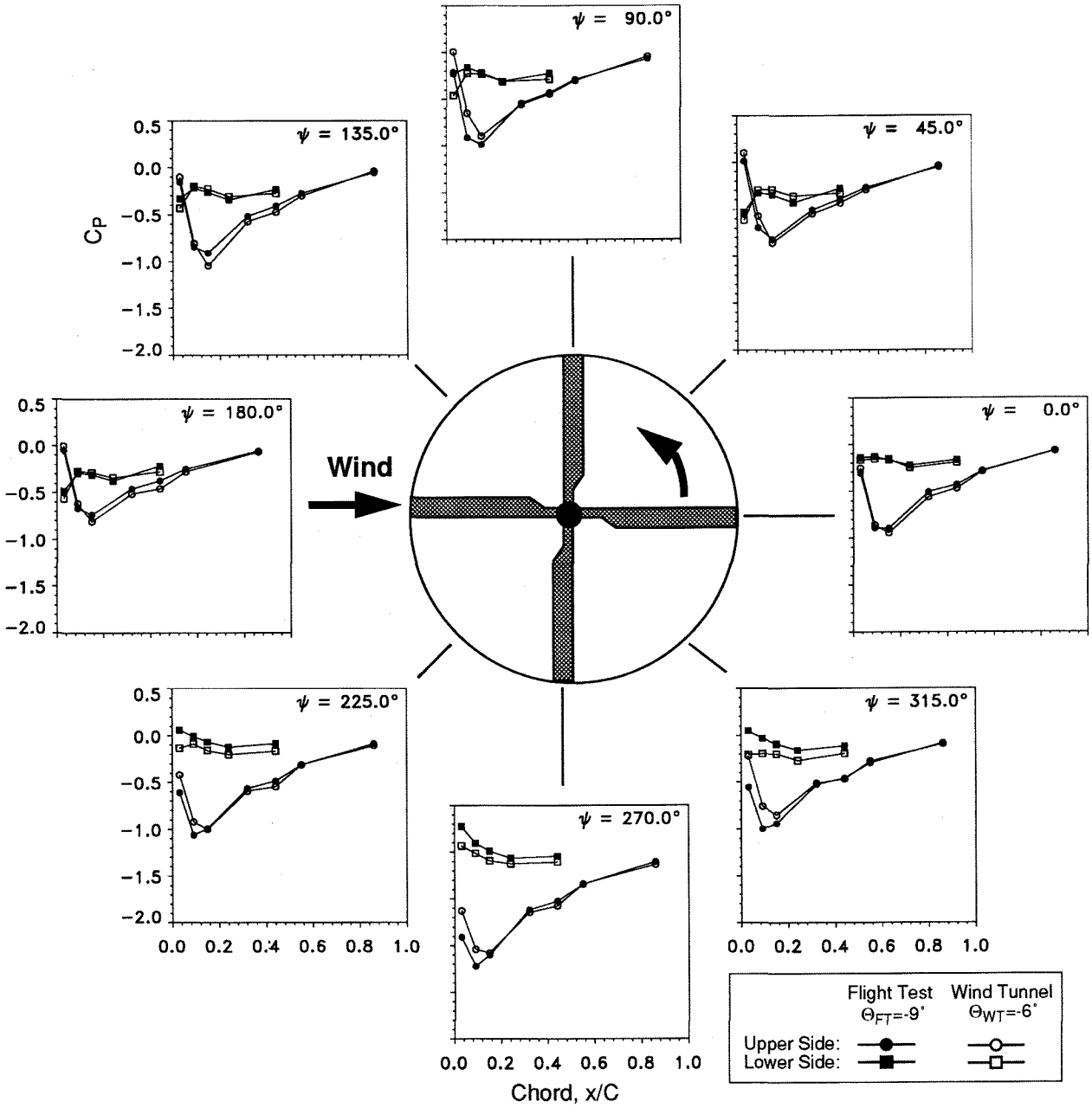

Fig. 15 Comparison of chordwise pressure distribution on the upper and lower blade surface at fixed rotor azimuthal positions (in 45°-steps) from wind tunnel (flight path angle = -6°) and flight (flight path angle = -9°) tests; V ≈ 32 m/s; $C_T \approx 0.0044$; $M_H \approx 0.641$

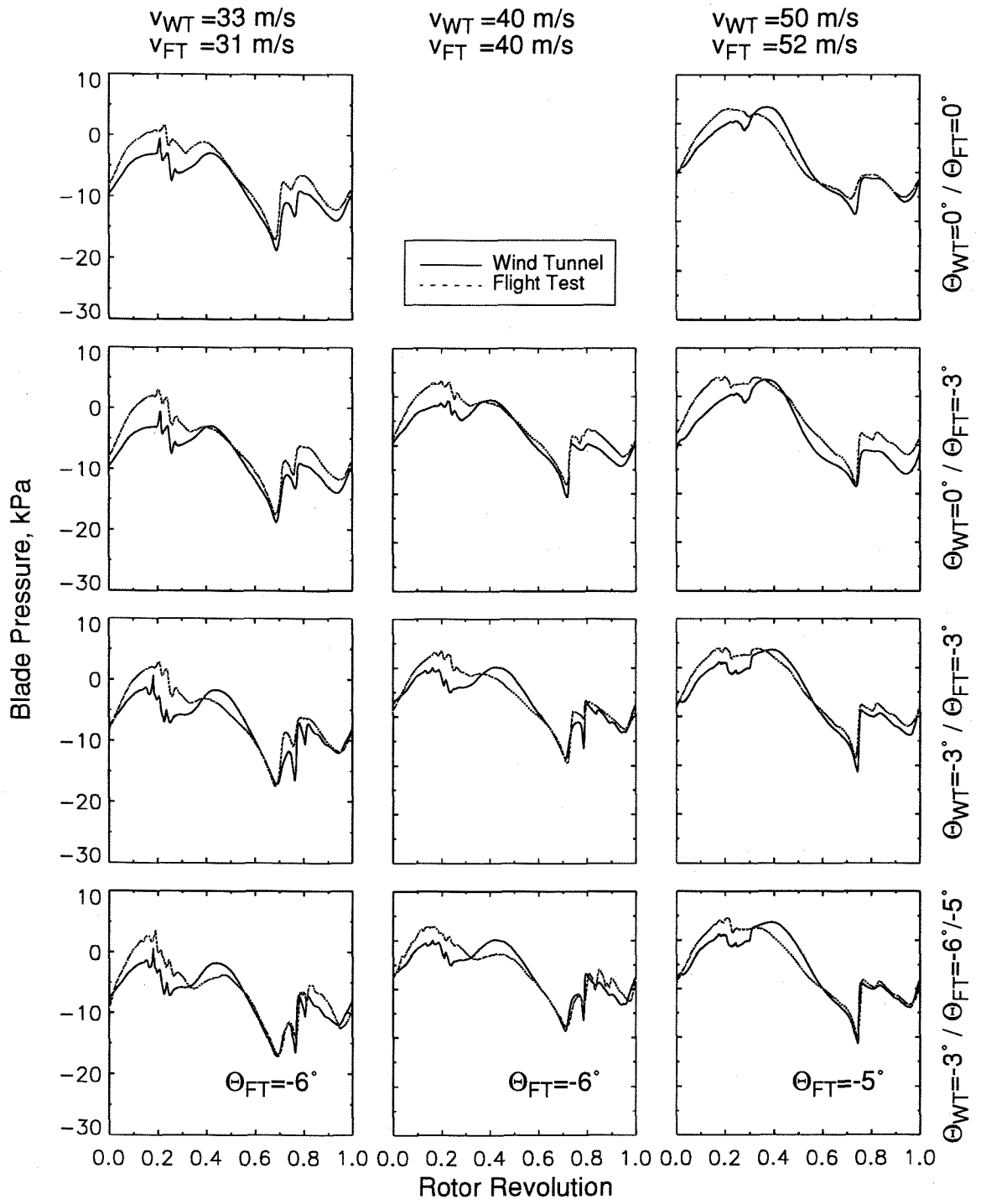

Fig. 16 Blade pressure time histories from wind tunnel and flight tests for an upper sensor location r/R = 87%, x/C = 3% at different flight path angles and speeds; $C_T \approx 0.0044$; $M_H \approx 0.641$

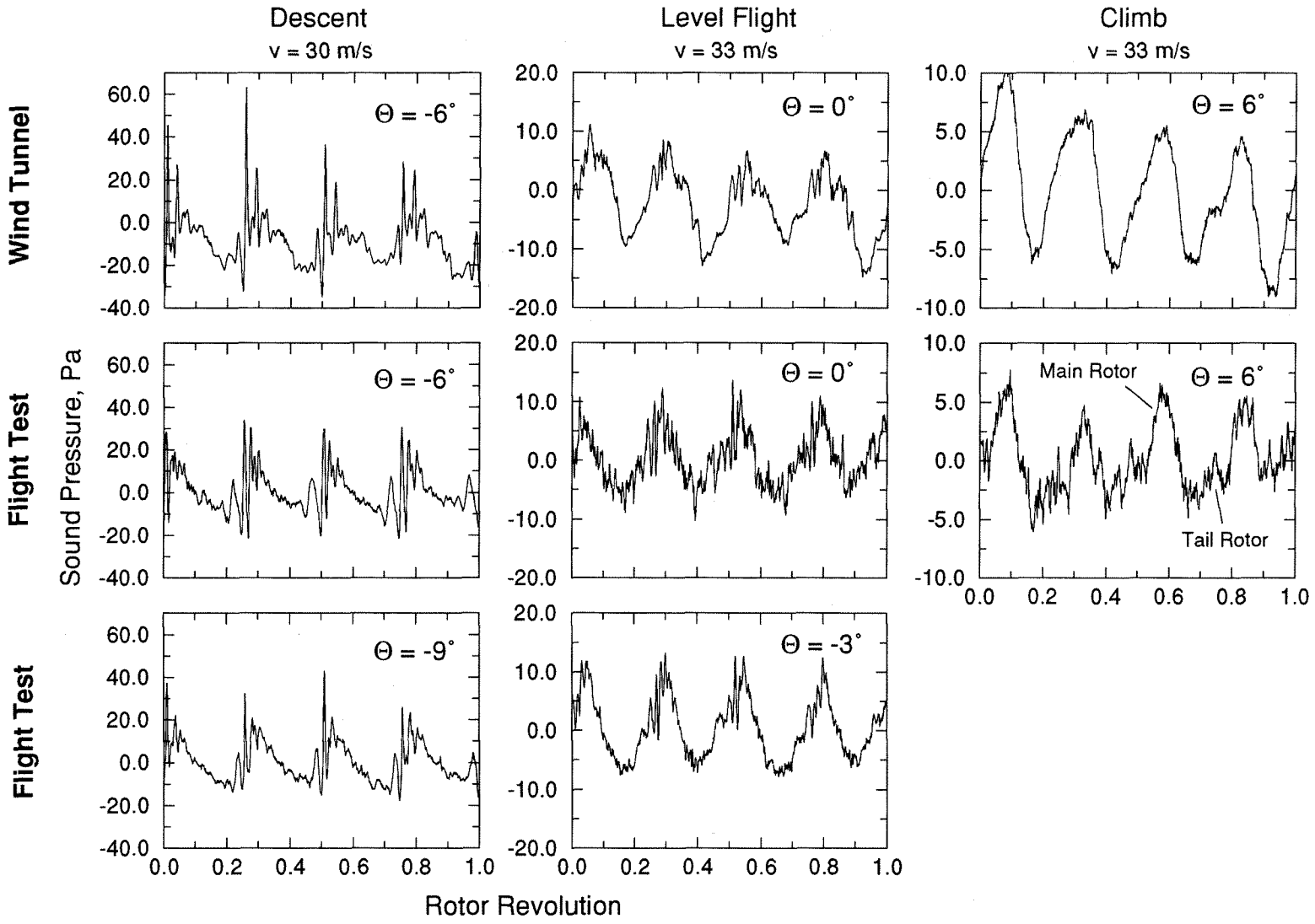

Fig. 17 Acoustic radiation from wind tunnel and flight tests at corresponding scaled locations under the advancing rotor side for one main rotor revolution for forward flight speeds from 30 to 33 m/s and conditions of descent, level flight and climb; $C_T \approx 0.0044$; $M_H \approx 0.641$

confirm the 3°-bias also for the acoustic radiation data. It should be noted that the absolute pressure amplitudes decrease from descent over level flight to climb, in that the peak-to-peak values vary from about 90 Pa for the descent condition to less than 20 Pa for the climb condition. Here, in the flight data pressure time histories over one main rotor revolution, depicting 4 main rotor related spikes, several of the tail rotor spikes (of which there are about 11 per one main rotor revolution) become visible.

4.3 Reasons for 3°-Flight Path Angle Bias

As described before, when comparing the blade pressure time histories of full-scale and model scale tests best agreement of the blade pressure signature shape is observed for conditions with a constant shift of about 3 degrees of the respective flight path angles. For example, the blade pressures signature for a 6 degree descent condition in the wind tunnel model test agrees best with that obtained for a 9 degree descent condition at the full-scale flight test, all other parameters being equal. This phenomenon was surprising and can not be fully explained at present. However some possible reasons are offered.

The most reliable indication for corresponding test conditions in model scale and full-scale should be the relevant rotor blade pressures. In a wind tunnel test the conditioning parameters can be measured with sufficient accuracy. In establishing a wind tunnel test condition, the important parameters advance ratio μ, tip path plane angle α'_{TPP} and thrust coefficient C_T are precalculated to match a desired full-scale flight condition using a force balance equivalency and a wind tunnel correction. The reason for differences in the wind tunnel and full-scale condition may be found in

1. the used formulation itself: The formulations for the force balance and for the wind tunnel correction are based on theory and there are several uncertainties involved. For an accurate correction of wind tunnel and flight results the ratio of lift and propulsive force should be identical in both cases. However, the drag component - to be overcome by the propulsive force - can only be estimated for the real helicopter. This is a source of error and may lead to a flight path angle bias of the order of 0.5 degrees.
2. not exactly corresponding test conditions: in flight tests it is quite difficult to exactly maintain the preselected conditions - forward speed, climb or descent rate, thrust coefficient C_T etc. Furthermore, the atmospheric conditions - wind gusts, air density, air temperature etc. - are usually also different from those under controlled wind tunnel conditions. An estimate of the effect of flight speed and C_T on the flight path angle can be made on the basis of the force balance equation

$$\Theta_{FT} - \alpha_{TPP} = 0.44\,\mu^2/C_T$$

A 10% lower speed and a 10% higher thrust - certainly possible uncontrollable deviations - would already result in a flight path angle deviation of about 0.6 degrees.

3. non-identical trim conditions: During the wind tunnel tests the rotor was operated with zero flapping. In a real flight the trim conditions are normally slightly different. This may result in a deviation of the shaft angle of perhaps up to 1 degree.
4. inaccurate measurements of the flight conditions: Measuring techniques for flight test purposes are not as exact as those employed in a wind tunnel experiment. Deviations of ±1 degree may readily occur; even a certain constant drift over time cannot be excluded.
5. rotor blades not being dynamically exactly scaled: Any difference in the aeroelastic properities of the model and the full-scale rotor blades could result in a different rotor dynamic behavior causing ever so small variations in the respective blade tip motions.

In total, differences of about 3 degrees are not improbable, but these should occur in a random fashion. Similar deviations had been observed in earlier comparisons of wind tunnel and flight test data [e.g. 2]. Still, it is not clear why the observed seemingly systematic deviation is obtained.

5. Conclusions

Recognizing that unsteady blade pressures on helicopter rotors constitute crucial information towards understanding the complex relationship of blade aerodynamics and acoustics, the full-scale flight tests, discussed in this report, provided important insight into the value of model-scale data to describe the complex aeroacoustics of a real helicopter rotor under actual flight conditions. The comparison of blade pressure characteristics obtained during the very comprehensive European HELINOISE project with those - admittedly still fairly limited ones - on the "full-scale counterpart rotor" (that of the BO-105 helicopter) nevertheless brought about the satisfying result that full-scale flight test data can indeed be reproduced in carefully executed model tests indicating a potential of a direct scalability (albeit from a fairly large, namely 40%-model). However, a conspicuous test-condition bias has been observed in that - for moderate flight speeds - model data agree best when compared with full-scale data of an approximately 3°-lesser angle. For example, the blade surface pressure time history on any given sensor location for a moderate speed (say, 32 m/s) descent condition with a flight path angle of minus six degrees agreed to within every minute detail to that observed on the same scaled sensor location of the full-scale rotor blade and the same flight speed, but for a flight path angle of minus nine degrees. That observation held true in the moderate flight speed range no matter whether a climb, a level flight or a descent condition was considered. Of course, that flight angle bias was not exact to the decimal point but it was clear, nevertheless, that its order of magnitude was about

3°±0.5°. Data suggested that at higher flight speeds this bias became smaller. In fact, at flight speeds around 50 m/s it seemed to vanish altogether. Unfortunately, the available data was not sufficient to fully confirm this observation, but the tendency seemed clear.

No clear-cut explanation can be given for the observed bias at this time, although several suppositions can be made. The most obvious - and least satisfactory - one might be that the rate-of-climb indicator on the aircraft provides incorrect values. However, all sorts of other distorting effects could be thought of, since the controlling parameter is not so much the flight path angle as such but rather the effective rotor tip path plane inclination towards the oncoming flow which should be different by that "magic" 3° in flight versus in the tunnel. If that was so, it could be that the tunnel flow corrections applied are inadequate since there are one or two empirical constants involved. Also there could be differences in the aeroelastic properties of the (after all) scaled model rotor with respect to its full-scale equivalent which could ultimately cause differences in the tip trajectory of the rotor blades.

These uncertainties need to be clarified. As a consequence, future flight tests (which indeed are planned) must be performed with an improved measuring system to exactly determine the prevailing flight condition. Furthermore, the flight tests must be made during stable atmospheric conditions (i.e. with as little wind as possible, and preferably air temperature and air density similar to the wind tunnel conditions). Finally, the force trim conditions for the model scale and full scale tests should be as close as possible (equal lift and propulsive force as well as equal flapping moments).

Accepting, for the time being, the bias, it is still surprising and satisfying that flight/wind tunnel operational conditions could be identified where respective blade pressure time histories show excellent agreement. Sometimes, however, inspite of the waveform agreement, a certain, albeit very minor, phase shift was observed in comparing full-scale and model-scale pressure time histories. This might again be caused by some of the reasons advanced above, but it could also be a result of a respectively different lead-lag behavior. Moreover, there might be small differences in the actual location of sensors at nominally "identical" positions. Some aeroacoustic phenomena on a rotor blade, most notably those related to the BVI-phenomenon are very localized ones, indeed, and any discrepancy in sensor location might have effects which are not insignificant.

It was observed that the actual flight path - as defined by flight speed and rate of climb (rate of descent) and hence the actual flight path angle - varied in a seemingly erratic manner. In fact, over several tens of rotor revolutions (i.e. 5 to 10 seconds of flight) the flight speed could vary by some 4% and the flight path angle by several degrees, even though the pilot was flying a "constant" flight path. This might be helicopter flight inherent, or caused by some ever present gusts. Accordingly, a novel data reduction approach was developed. Originally it had been attempted to average pressure time histories over several tens of rotor revolutions, resulting however, in extremely scattered data which is understandable on account of the "erratic" flight paths. Therefore, a search algorithm was developed where individual one-time-rotor-revolutions were identified for which a particular flight condition was exactly met, or met within a defined small tolerance. Within a given measurement flight, such a condition could be met very few times, or relatively often. In any case, these then "identical" individual rotor revolutions were taken as the basic data set for that flight condition and averaged. This way "good" flight data was obtained for comparison with data from the wind tunnel (whose operational parameters could of course be much better controlled). This procedure turned out as being very feasable.

In summary then, the following statements - and answers to the questions posed in the introduction to this paper - may be made and given:

- The excellent agreement of blade pressure waveforms confirms that a match of flight and wind tunnel operational parameters should be possible; this statement is not contradicted by the - presently still not fully explained - observed bias of several degrees in the effective tip path planes for the tunnel and the flight test at moderate flight speeds, since better agreement seems to exist at higher flight speeds. Certainly, this existing inconsistency must be resolved.

- It seems that a precise matching of wind tunnel and flight operational parameters is essential for highly localized aerodynamic/acoustic phenomena such as occurring during blade/vortex interactions (and presumably also for conditions of high speed impulsive noise where shocks appear on the blade surfaces; such conditions however could not be attained during the subject flight test program). If such highly localized phenomena are absent, then exact matching might not be so critical.

- Agreement of flight and wind tunnel data is excellent given the relatively small number of sensor locations and flight conditions for which comparisons were possible. For example, each individual spike - both in time and amplitude - of a sequence of blade vortex interactions could be duplicated. Acoustic data (sound radiation) seems to agree quite well too, it being seemingly less sensitive to minor differences in the test/operational conditions.

The tests served to significantly further the understanding of realistic rotor aeroacoustic phenomena and of the reliability of model-scale tests versus the full-scale flight situation. This flight test program was a start in the attempt to validate results of the numerous previous experimental rotor aeroacoustics programs in the DNW conducted so far and will help in the execution and inter-

pretation of future similar tests presently being in the planning stage.

Acknowledgements

The authors thank Daniela Fischer for her assistance in the data reduction. They appreciate the help of Horst Meyer and Rainer Holland of the DLR Institute of Flight Mechanics in preparing the flight-worthy hardware of the data acquisition system, and last not least the dedication of the DLR-pilots, Manfred Rössing and (the late) Klaus Sanders of the DLR Flight Division.

References

[1] Boxwell, D., Schmitz, F., Splettstoesser, W. R., Schultz, K.-J.; "Model Helicopter Rotor High Speed Impulsive Noise - Measured Acoustics and Blade Pressures", NASA Tech. Memo 85850 and US-AAVRADCOM Tech. Report 83-A-14, Sep. 1993

[2] Splettstoesser, W. R., Schultz, K.-J., Boxwell, D., Schmitz, F.; "Helicopter Model Rotor Blade/Vortex Interaction Impulsive Noise - Scalability and Parametric Variations", 10th European Rotorcraft Forum, The Hague, Aug. 1984 and NASA Tech. Mem. 86007, TM-84-A-7

[3] Dadone, L., Dawson, S., Boxwell, D., Ekquist, D.; "Model 360 Rotor Test at DNW - Review of Performance and Blade Airload Data", AHS 43rd Annual Forum, St. Louis, MI, May 1987

[4] Zinner, R., Boxwell, D., Spencer, R.; "Review and Analysis of the DNW Model 360 Rotor Acoustics Data Base", 15th European Rotorcraft Forum, Amsterdam, Sep. 1989

[5] Schultz, K.-J., Splettstoesser, W. R.; "Model Tail Rotor Noise Study in the DNW - Measured Acoustics, Blade Pressures, Noise Predictions", Paper No. 78, Proceedings, 18th European Rotorcraft Forum, Avignon, Sep. 1992

[6] Liu, R. S., Marcolini, M.A.; "The Acoustic Results of the United Technologies' Scale Model Helicopter Rotor Tested at the DNW", AHS 46th Annual Forum, Washington D.C., May 1990

[7] Lorber, P.F.; "Aerodynamic Results of a Pressure Instrumented Model Rotor Test at the DNW", AHS 46th Annual Forum, Washington D.C., May 1990

[8] Polacsek, C., Lafon, P.; "High-Speed Impulsive Noise and Aerodynamic Results for Rectangular and Swept Rotor Blade Tip Tests in S1-Modane Wind Tunnel", Paper 91-60, 17th European Rotorcraft Forum, Berlin, 1991

[9] Isaacs, N. C. G., Harrison, R. J.; "Identification of Retreating Side Blade Stall Mechanisms Using Flight Test Pressure Measurements" AHS 45th Annual Forum, Boston, May 1989

[10] Kufeld, R. M., Balough, D. L., Cross, J. L., Studebaker, K. F., Jennison, C. D., Bousman, W.G.; "Flight Testing the UH-60A Airloads Aircraft", AHS 50th Annual Forum, Washington D.C., May 1994

[11] Splettstoesser, W. R. , Niesl, G., Cenedese, F., Papanikas, D., Nitti, F.; "Experimental Results of the European HELINOISE Aeroacoustic Rotor Test in the DNW", Paper No. B8, Proceedings, 19th European Rotorcraft Forum, Cernobbio, Italy, Sep. 1993

[12] Splettstoesser, W. R., Junker, B., Schultz, K.-J., Wagner, W., Weitemeyer, W., Protopsaltis, A., Fertis, D.; "The HELINOISE Aeroacoustic Rotor Test in the DNW - Test Documentation and Representative Results", DLR Mitteilung 93-09, Dec. 1993

[13] Heller, H., Splettstoesser, W. R. , Kloeppel, V., Cenedese, F.: "HELINOISE - The European Community Rotor Acoustics Research Program", AIAA 93-4358, 15th AIAA Aeroacoustics Conference, Long Beach, CA, Oct. 1993

[14] Van Ditshuizen, J. C. A., Courage, G. D., Ross, R., Schultz, K.-J.; "Acoustic Capabilities of the German Dutch Wind Tunnel (DNW)", AIAA-83-0146, Jan. 1983

[15] Stephan, M., Kloeppel, V., Langer, H.-J.; "A New Wind Tunnel Test Rig for Helicopter Testing", Paper No. 66, 14th European Rotorcraft Forum, Sep. 1988

[16] Heyson, H. H.; "Use of Superposition in Digital Computers to obtain Wind Tunnel Interference Factors for Arbitrary Configurations, with particular Reference to V/STOL Models", NASA TR R-302, 1969

[17] Brooks, T. F., Jolly, R.J., Marcolini, W.R.; " Determination of Noise Source Contributions using scaled Model Rotor Acoustic Data" NASA TP 2825, 1988